International Journal of Biological Macromolecules 163 (2020) 358–365

Contents lists available at ScienceDirect

International Journal of Biological Macromolecules

journal homepage: http://www.elsevier.com/locate/ijbiomac

Facile strategy for immobilizing horseradish peroxidase on a novel acetate functionalized ionic liquid/MWCNT matrix for electrochemical biosensing

K. Theyagarajan, Mari Elancheziyan, Prakash Sinha Aayushi, Kathavarayan Thenmozhi *

Department of Chemistry, School of Advanced Sciences, Vellore Institute of Technology (VIT), Vellore 632014, India

ARTICLE INFO

Article history:
Received 16 May 2020
Received in revised form 24 June 2020
Accepted 2 July 2020
Available online 04 July 2020

Keywords:
Ionic liquid
Electrochemical biosensor
Horseradish peroxidase
Direct electrochemistry
Hydrogen peroxide
MWCNT

ABSTRACT

Facile yet simple platforms for the immobilization of biomolecules have always been a substantial requirement for the fabrication of proficient biosensors. In this study, we report a naphthyl substituted acetate functionalized ionic liquid (NpAc-IL) for the covalent anchoring of horseradish peroxidase (HRP), using which the direct electrochemistry of HRP was successfully accomplished and a H_2O_2 biosensor was developed. The naphthyl substitution on the NpAc-IL was utilized for the π-π stacking with the MWCNT modified GCE and the terminal -OCH_3 group of NpAc-IL was used for the covalent attachment with the free -NH_2 group of HRP via amide bond formation. High conducting nature of the newly designed ionic liquid (NpAc-IL), facilitated an improved communication with the deeply buried redox centre of the HRP, while the covalent bonding provided enhanced stability to the fabricated biosensor by stably holding the water soluble HRP enzyme on the electrode surface. Furthermore, incorporation of MWCNT on the sensor setup synergistically enhanced the sensitivity of the developed biosensor. Under optimized conditions, the fabricated biosensor showed an enhanced electrocatalytic reduction of H_2O_2 in the range of 0.01 to 2.07 mM with a limit of detection and sensitivity of 2.7 μM and 55.98 μA mM^{-1} cm^{-2} respectively. Further, the proposed biosensor was utilized for the sensing of H_2O_2 spiked in real samples. Moreover, the newly fabricated biosensor demonstrated excellent stability with improved sensitivity and selectivity towards H_2O_2 reduction. The superior analytical characteristics are attributed to the facile fabrication strategy using this newly developed acetate functionalized ionic liquid platform.

1. Introduction

Sensitive and selective determination of trace analytes in a complex system is highly challenging and thus there is always a persuasive need to develop facile and affordable analytical techniques [1,2]. Electrochemical sensors and biosensors play an attractive role in virtue of their simplicity, selectivity, rapid response towards the target analytes, ease of handling and the ability to scale down an extended and complicated system in a much simpler way [3–5]. The choice of electrode material is of paramount importance in determining the performance of fabricated sensors and biosensors and thus researchers have designed and utilized various advanced materials and molecules to improve the performance of the sensors in terms of electronic conductivity, sensitivity, stability, etc. [6–10]. These nonenzymatic sensors have the advantages of easy fabrication, high storage stability and so on, whereas their selectivity is a major concern [11,12]. The selectivity issue could be surpassed by the utility of suitable enzymes and the electrochemical enzymatic biosensors are highly selective towards the target analytes even in a highly complex reaction mixture or real sample solution [13,14]. Holding the biomolecules on the electrode surface and accessing their redox centres while preserving their nativity in the biosensor setup is a predominant criterion for any fabricated biosensor [15–19]. Significant efforts have been taken to develop enzyme nanoflowers in order to address the issues associated with immobilized enzymes [20–25]. Several organic-inorganic based new materials with enzyme mimicking activity were reported with impressive performances [26–28]. Further, carbon nanomaterials, metallic and bimetallic nanoparticles, redox mediators, ionic liquids, etc. were incorporated in the electrode setup to improve the conductivity as well as the performance of the biosensors effectively. However, the design of novel materials or new combinations of these materials is still demanding in order to develop facile platforms to ensure the desirable performance of these biosensors at device levels.

Multiwalled carbon nanotubes (MWCNTs) are an important class of nanomaterials, which have improved electronic properties as compared to other materials along with excellent chemical and mechanical stabilities as well as larger surface area. They could be effectively stacked on the surface of the electrodes along with various electrode modifiers through their π electron clouds, which could concurrently improve the

* Corresponding author.
E-mail addresses: k.thenmozhi@vit.ac.in, kt.thenmozhi@gmail.com (K. Thenmozhi).

https://doi.org/10.1016/j.ijbiomac.2020.07.005
0141-8130/

conductivity [29–31]. On the other hand, ionic liquids (ILs) also have drawn tremendous attention due to their fascinating characteristics which include enhanced ionic conductivity, good electrochemical stability and improved biocompatibility along with negligible vapour pressure [32–34]. They possess good synthetic versatility and can be rationally designed and synthesized depending on the need as well as for task specific applications [35,36]. These characteristics enable ILs as strong candidates towards the development of platforms for electrochemical biosensing [37–39]. Therefore, integration of ILs together with MWCNTs in the modified electrode set up could afford multifaceted benefits. However, physical immobilization of biomolecules with MWCNTs or ILs may result in leaching of biomolecules from the modified surface, which would diminish the performance of the biosensor. Thus, covalent immobilization of these biomolecules on suitably designed IL matrix could be a better methodology for the effective anchoring of biomolecules, which would enhance its stability as well as the electrocatalytic performance.

In our previous studies, amine and carboxylic acid functionalized ionic liquids were synthesized and utilized for the covalent linking of hemoglobin and cytochrome *c* through appropriate crosslinkers [40,41]. In our continuous strive on different IL based platforms, we further intended to simplify the biosensor fabrication, wherein the biomolecule could be immobilized on the IL directly without any crosslinker. This motivated us to synthesize an acetate functionalized IL for the direct immobilization of enzyme through amidation reaction and to explore its efficacy towards biosensing. H_2O_2 is a versatile reagent and a multipurpose chemical, which finds variety of applications in arenas of pharmaceutical, food, paper and textile industries as well as plays varied roles in clinical and domestic purposes. Excess concentrations of H_2O_2 in the biological system causes diseases varying from simple irritations to life threatening conditions like apoptosis, Parkinson's disease, Alzheimer's disease and even cancer [42,43]. Horseradish peroxidase (HRP) is a simple heme containing metalloenzyme and commonly used redox enzyme for the selective determination of H_2O_2 [44,45].

In the present work, we have strategically designed and synthesized a naphthyl substituted acetate functionalized ionic liquid (NpAc-IL) and explored its efficacy as a platform for the direct immobilization of HRP enzyme and to develop a H_2O_2 biosensor. The naphthyl substitution on the NpAc-IL was utilized for the π-π stacking on MWCNT/GCE and the terminal -OCH_3 group of NpAc-IL was used for amide bond formation with HRP. Moreover, the deeply buried redox centre of the HRP was accessed and the direct electrochemistry of HRP was successfully achieved. Covalent immobilization of HRP on NpAc-IL/MWCNT/GCE matrix facilitated an improved conductivity and an enhanced stability to the fabricated biosensor. Thus, fabricated HRP-NpAc-IL/MWCNT/GCE biosensor was utilized for the enzymatic determination of H_2O_2 and showed an excellent stability with improved sensitivity and selectivity.

2. Experimental

2.1. Chemicals and materials

Imidazole (≥99%), 1-chloromethyl naphthalene (≥97%), sodium hydride (NaH, 60% in mineral oil), methyl bromoacetate (97%), potassium hexafluorophosphate (KPF_6, ≥99%), MWCNT (>98%) were procured from Sigma-Aldrich, India. Peroxidase ex. horseradish (HRP), NaH_2PO_4 (99%) and Na_2HPO_4 (99%) were received from Sisco Research Laboratories, India. Hydrogen peroxide (30%) was procured from Merck, India. Other reagents and solvents were of analytical reagent (AR) grade and used as purchased. Glassy carbon electrode (GCE) with 0.071 cm^2 geometric area was received from CH Instruments. Milli-Q water obtained from Millipore water system (resistivity 18.2 MΩ cm at 25 °C) was utilized for the preparation of phosphate buffer (0.1 M, pH 7.0) solutions using NaH_2PO_4 and Na_2HPO_4. All the electrochemical experiments were performed at room temperature (RT) and, the fabricated biosensor was stored at 4 °C.

2.2. Instrumentation

FTIR (Fourier transform infrared) spectral studies were conducted in Shimadzu, IR Affinity-1 FTIR spectrophotometer using ATR (Attenuated total reflectance) mode between the wavenumbers 4000 and 400 cm^{-1} to measure the functional changes occurring in the molecules. NMR (Nuclear magnetic resonance) spectra were performed in Bruker, Ascend (400 MHz) spectrometer using the deuterated DMSO-d_6 solvent. The chemical shift (δ) values were represented in ppm against TMS ($\delta = 0.0$) as the internal reference and spectra were interpreted using Topspin 4.0.5 software. HRMS (High-resolution mass spectrometry) spectrum was recorded in JEOL (GC Mate-II) spectrometer by electron impact ionization (70 eV) method. Cyclic voltammetry (CV) and amperometry were carried out using CHI 620E electrochemical workstation from CH Instruments (Austin, Texas). EIS (electrochemical impedance spectroscopy) was performed in Autolab PGSTAT 204 potentiostat from Metrohm, Netherlands. A customary three-electrode system comprising of unmodified or modified GCE as working electrode, platinum coil as the auxiliary electrode and Ag/AgCl as reference electrode was utilized for electrochemical studies. Electrochemical measurements such as CV and amperometry were performed under nitrogen saturated phosphate buffer solution (0.1 M, pH 7.0).

2.3. Synthesis of naphthyl substituted acetate functionalized ionic liquid

Naphthyl substituted acetate functionalized ionic liquid (NpAc-IL) has been synthesized in the following steps and the stepwise synthesis is presented in Fig. 1.

2.3.1. Synthesis of 3-(2-methoxy-2-oxoethyl)-1-(naphthalen-1-ylmethyl)-1H-imidazol-3-ium bromide

Initially, 1-naphthylmethylimidazole was dissolved in acetonitrile and constantly stirred at RT. To the above solution, methyl bromoacetate dissolved in acetonitrile was added slowly under same condition and the resulting mixture was refluxed at 75 °C, for 20 h. After completion of the reaction, solvent was removed by evaporation and the residue was washed with ethyl acetate, followed by diethyl ether, yielding naphthyl substituted acetate functionalized ionic liquid with bromide counter anion.

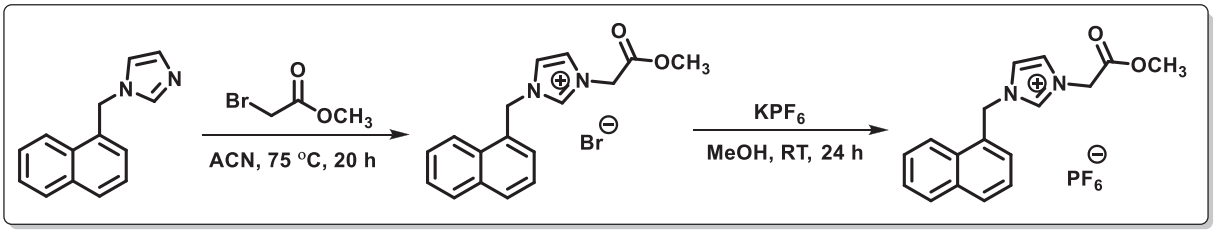

Fig. 1. Scheme for the synthesis of NpAc-IL.

2.3.2. Synthesis of 3-(2-methoxy-2-oxoethyl)-1-(naphthalen-1-ylmethyl)-1H-imidazol-3-ium hexafluorophosphate (NpAc-IL)

NpAc-IL obtained with bromide anion is water soluble and hence anion exchange was carried out with potassium hexafluorophosphate to make it water insoluble NpAc-IL. A methanolic solution of KPF_6 was added to a constantly stirred methanolic solution of bromide anion based NpAc-IL and the stirring continued at RT for 24 h. After the reaction, MeOH was removed under vacuum and the obtained residue was washed with dry diethyl ether, then dried to furnish water insoluble PF_6^- anion based NpAc-IL with 88% yield. ^{1}H NMR (400 MHz, DMSO-d_6): δ 3.71 (s, 3H, O-CH_3), 5.22 (s, 2H, -CH_2-CO-), 6.02 (s, 2H, Ar-CH_2-), 7.53–7.62 (m, 4H), 7.76 (s, 1H), 7.86 (s, 1H), 8.02–8.04 (d, 2H), 8.12–8.13 (d, 1H). 9.19 (s, 1H, acidic imidazolium) ppm. ^{13}C NMR (100 MHz, DMSO-d_6): δ 50.14, 50.50, 53.27, 123.08, 123.33, 124.61, 126.13, 126.96, 127.71, 128.16, 129.39, 130.24, 130.41, 130.89, 133.94, 138.02, 167.77 ppm. ^{31}P NMR (162 MHz, DMSO-d_6) δ −157.38, −152.98, −148.59, −144.20, −139.81, −135.43, −131.03 ppm. ^{19}F NMR (376 MHz, DMSO-d_6) δ −71.07, −69.18 ppm. HRMS (EI): $[C_{17}H_{17}N_2O_2]^+$, calculated mass (281.3345), obtained (281.3342).

2.4. Fabrication of HRP-NpAc-IL/MWCNT/GCE biosensor

Alumina slurries of different grades were used for polishing the GCE and then ultrasonicated in ethanol and water (1:1) mixture for 3 min. After drying at RT, 5 μL ethanolic solution of MWCNT (1 mg/0.5 mL) was dropcasted on the GCE to prepare MWCNT/GCE. Further, 5 μL methanolic solution of NpAc-IL (2 mg/100 μL) was immobilized on MWCNT/GCE to form a π-π stacking of naphthalene ring of IL over the π-conjugations of MWCNT modified GCE. After drying at RT, HRP was covalently immobilized by dropcasting 5 μL (1 mg/100 μL) of it on NpAc-IL-MWCNT/GCE and incubated for 2 h to form HRP-NpAc-IL/MWCNT/GCE, which forms a stable amide bond by the reaction between the -OCH_3 of NpAc-IL and free -NH_2 of HRP. The developed sensor was washed thoroughly with copious amount of phosphate buffer in order to eliminate the unbound enzymes on the fabricated biosensor. For comparison, HRP-NpAc-IL/GCE (without MWCNT) was also fabricated by following a similar strategy. The loading of MWCNT, NpAc-IL and HRP during the fabrication of biosensor were optimized and the details are presented in the Supplementary information (Fig. S4).

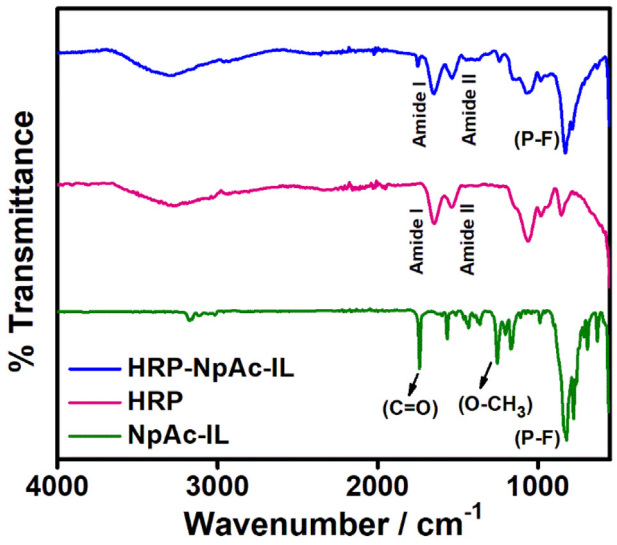

Fig. 3. FTIR comparison spectra of NpAc-IL (Green), HRP (Magenta), HRP-NpAc-IL (Blue).

3. Results and discussion

The synthesis of naphthyl substituted acetate functionalized ionic liquid in different steps was monitored using ^{1}H, ^{13}C, ^{31}P & ^{19}F NMR and mass spectroscopy techniques (Figs. S1–S3). The NpAc-IL on MWCNT was employed as a platform towards the direct covalent linking of HRP. The acetate functionality on the NpAc-IL was utilized for covalent immobilization with free amino groups of the HRP enzyme and naphthyl ring for the π-π stacking with the MWCNT. Fabrication of the modified electrode has been demonstrated stage by stage in Fig. 2.

3.1. Covalent immobilization of horseradish peroxidase on NpAc-IL

The covalent immobilization of HRP on NpAc-IL was characterized by FTIR spectral analysis and is shown in Fig. 3. The green curve represents the synthesized NpAc-IL, which shows C═O stretching frequency

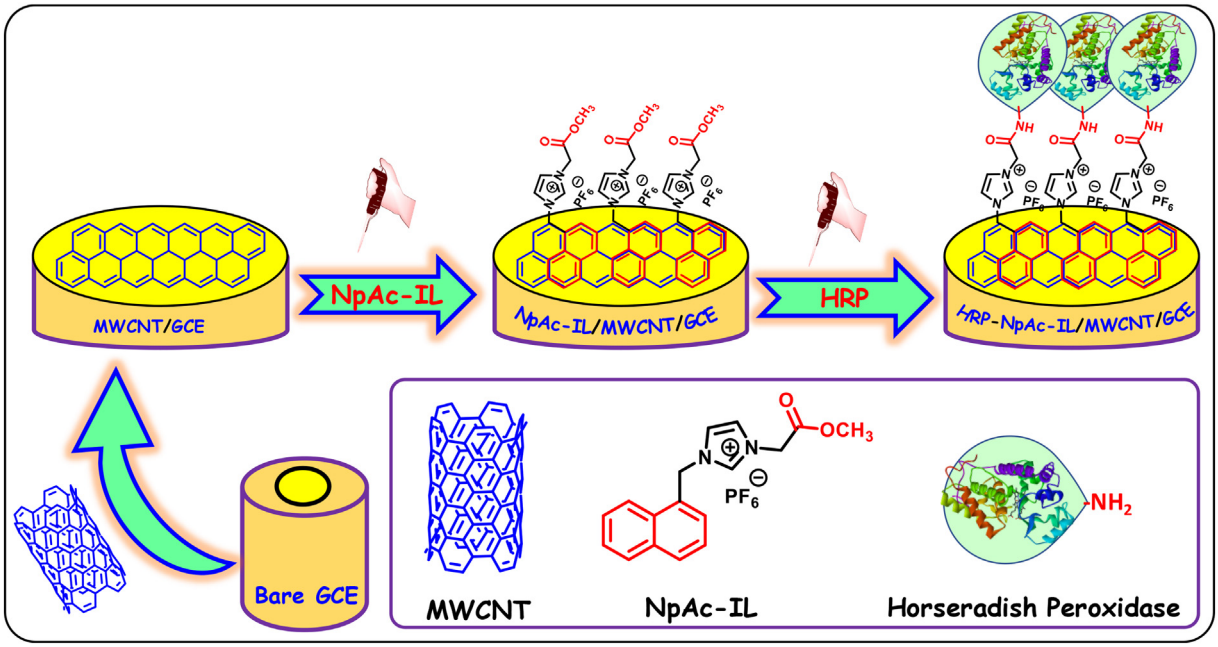

Fig. 2. Stepwise fabrication of HRP-NpAc-IL/MWCNT/GCE biosensor.

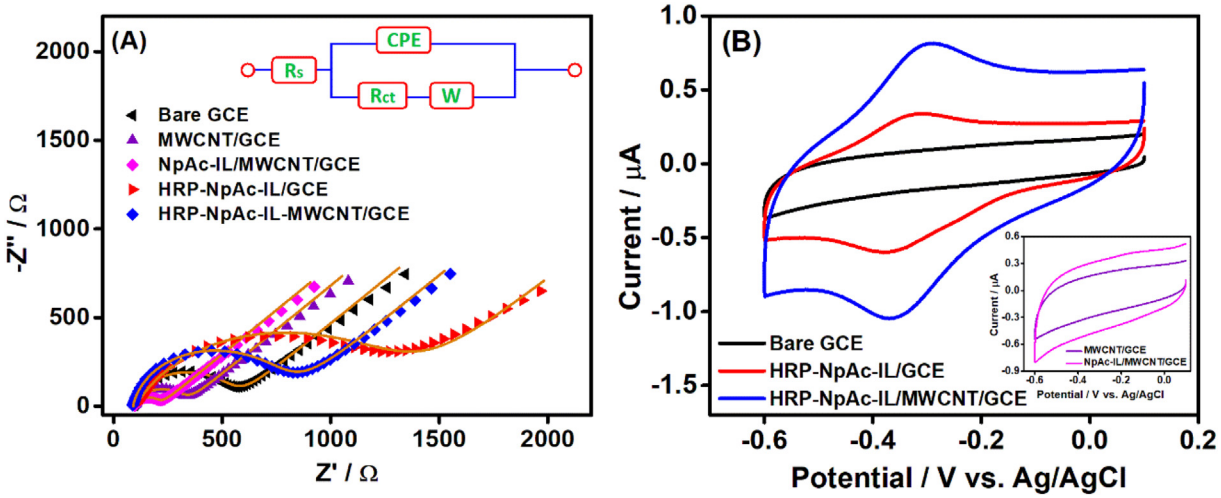

Fig. 4. (A) Nyquist plots of Bare GCE (Black), MWCNT/GCE (Violet), NpAc-IL/MWCNT/GCE (Pink), HRP-NpAc-IL/GCE (Red) and HRP-NpAc-IL/MWCNT/GCE (Blue) in 2.5 mM $[Fe(CN)_6]^{3-/4-}$ solution in 0.1 M KCl obtained during fabrication. Inset: Equivalent circuit and (B) CVs of stepwise fabricated biosensor of bare GCE (Black), MWCNT/GCE (Violet), NpAc-IL/MWCNT/GCE (Pink), HRP-NpAc-IL/GCE (Red) and HRP-NpAc-IL/MWCNT/GCE (Blue) (Scan rate: 50 mV s^{-1}).

at 1735 cm^{-1} and -OCH_3 stretching as three vibration bands around 1250–1160 cm^{-1} which confirms the presence of acetate group on NpAc-IL [46]. The peak around 830 cm^{-1} confirms the presence of P–F stretching frequencies of hexafluorophosphate anion in NpAc-IL. FTIR of native HRP shows (magenta curve) amide I and II stretching vibrations around 1643 cm^{-1} and 1542 cm^{-1}, respectively [47]. Upon the covalent linking of HRP on NpAc-IL via amide bond formation between the -NH_2 group of HRP and free -OCH_3 group of NpAc-IL as shown in blue curve, there is a disappearance of -OCH_3 stretching vibrations of NpAc-IL with a little broadening of amide I peak which indicates the covalent bonding. Moreover, appearance of amide I and II peaks of HRP depicts that the enzyme retains its secondary structures as well as preserves its nativity even after being covalently attached to NpAc-IL. FTIR spectral results demonstrate the successful covalent linking of HRP enzyme on the newly synthesized NpAc-IL, which serves as an anchoring site as well as provides a biocompatible microenvironment for the enzyme immobilization.

3.2. Electrochemical impedance spectroscopy (EIS)

EIS is an effective tool to study the impedance changes between the electrode and electrolyte interface, which helps in understanding the interface properties of the fabricated biosensor and the EIS results are shown as Nyquist plots in Fig. 4A. The EIS results of different modified electrodes are displayed as a linear part and a semicircle part, whose diameter correspond to the charge transfer resistance (R_{ct}). The results obtained data were fitted with a Randle's circuit and shown as inset to Fig. 4A. The EIS of bare GCE (black) showed a R_{ct} of 526 Ω indicating a poor redox process of the unmodified electrode in 0.1 M KCl containing 2.5 mM $[Fe(CN)_6]^{3-/4-}$ solution. After the incorporation of MWCNT (MWCNT/GCE, violet), the R_{ct} reduced to 293 Ω which denotes the high conducting nature of MWCNT. Further, immobilization of NpAc-IL on MWCNT/GCE (NpAc-IL/MWCNT/GCE, pink) through π-π stacking over MWCNT, enhances the conductivity (low resistance) and shows a lowest R_{ct} of 165 Ω. Covalent immobilization of HRP on the NpAc-IL/GCE (HRP-NpAc-IL/GCE, red) was confirmed by the predominant increase in the R_{ct} to a largest value of 1333 Ω, which significantly reduced to 802 Ω after the incorporation of MWCNT (HRP-NpAc-IL/MWCNT/GCE, blue) into the biosensor setup. EIS results substantiate that the newly developed NpAc-IL/MWCNT/GCE matrix provides enhanced conductivity, which facilitates the rapid electron shuttling for the immobilized biomolecules at the electrode surface.

3.3. Direct electrochemistry of HRP and electrocatalytic behaviour of HRP-NpAc-IL/MWCNT/GCE towards H_2O_2 biosensing

The stepwise fabrication of the modified electrode was characterized by recording their CV between the potential window of 0.1 V and − 0.6 V in N_2 saturated 0.1 M phosphate buffer solution (scan rate: 50 mV s^{-1}) and the corresponding CVs are shown in Fig. 4B. The black, violet and pink curves represent the voltammetric response of bare GCE, MWCNT/GCE and NpAc-IL/MWCNT/GCE, respectively. There are no obvious redox peaks within the potential window studied, revealing the non-redox nature of the bare GCE, MWCNT/GCE and NpAc-IL/MWCNT/GCE. After covalent immobilization of HRP on NpAc-IL/GCE (HRP-NpAc-IL/GCE, red curve), an apparent redox peak appeared with a formal potential ($E°$) of −0.34 V, which corresponds to the Fe^{III}/Fe^{II} redox centre of the HRP enzyme [48], shown in Eq. (1).

$$\mathrm{HRP}\left(\mathrm{Fe^{III}}\right) + \mathrm{H^+} + \mathrm{e^-} \leftrightarrow \mathrm{HRP}\left(\mathrm{Fe^{II}}\right)\ (\text{Direct Electron Transfer}) \qquad (1)$$

This gives an evidence about the high conducting and biocompatible nature of the rationally synthesized NpAc-IL, which effectively communicates the signal received from the deeply buried redox centre of the enzyme as well as preserves the activity of the covalently immobilized HRP enzyme. Moreover, incorporation of MWCNT in the fabrication of biosensor (HRP-NpAc-IL/MWCNT/GCE, blue curve), enhanced both the peak currents and also the $E°$ sufficiently reduced to −0.32 V. CV investigations revealed the high conducting and biocompatible environment of the developed NpAc-IL/MWCNT/GCE matrix for the effective covalent anchoring of the HRP enzyme, which could ultimately provide a facile environment and improve the efficiency of the developed biosensor.

The effect of pH on the fabricated biosensor was investigated from pH 5 to 9 in 0.1 M phosphate buffer solution (Fig. S5). On increasing the pH from 5 to 7, there was a steady increase in the cathodic peak current, which further reduced as the pH changes from 7 to 9. The results denote that maximum electrochemical behaviour of the fabricated biosensor could be attained at physiological conditions (pH 7.0) and therefore, neutral pH was chosen as the optimum condition for the electrochemical studies. Similarly, the effect of temperature on the fabricated biosensor was investigated in the temperature range from 15 to 50 °C (Fig. S6). Since, the current response was maximum and similar in the temperature range from 25 to 35 °C, we have chosen 25 °C (RT) as the optimum temperature for further experiments. Further, the effect of scan rate on the fabricated biosensor was performed from 10 to

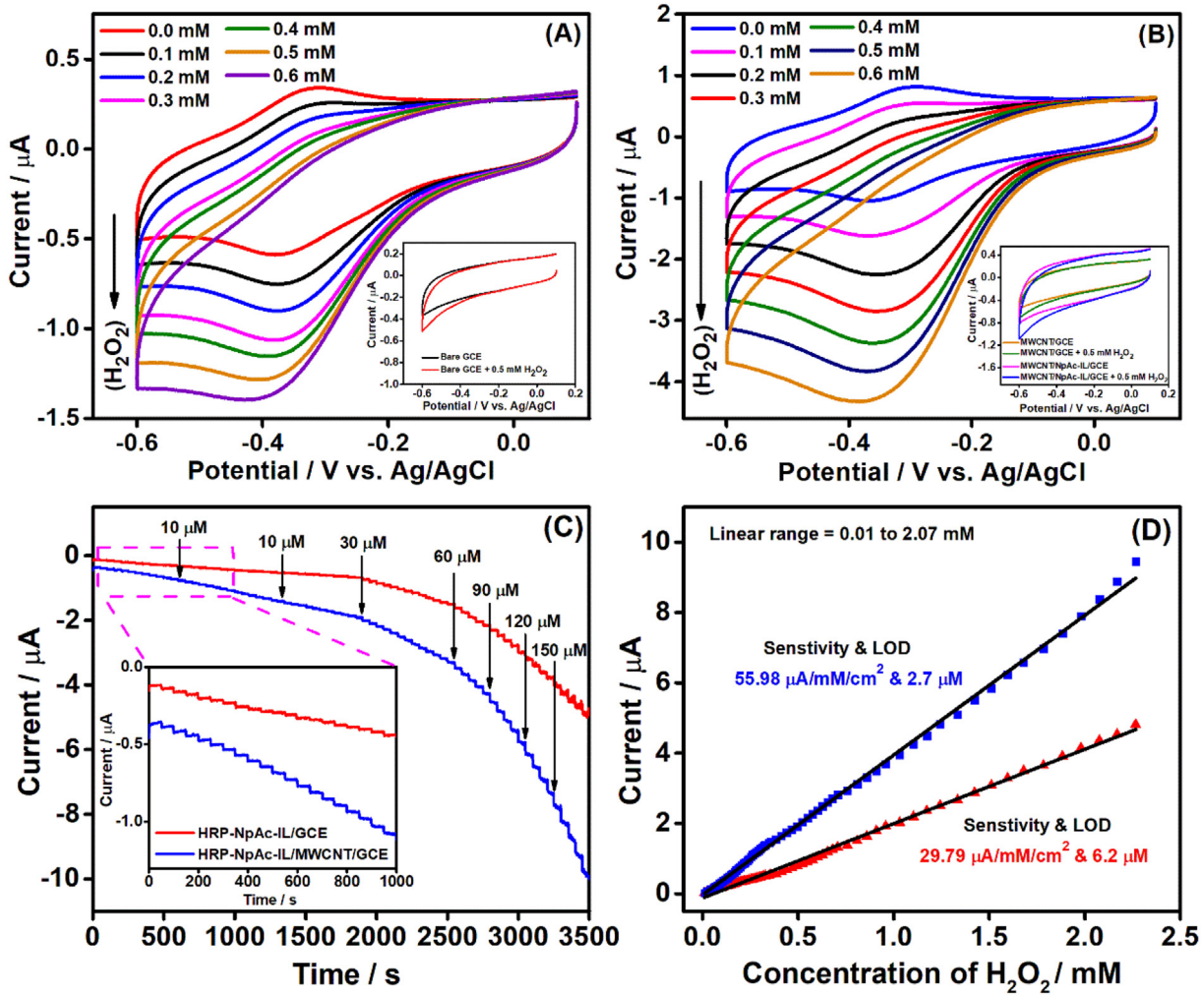

Fig. 5. (A) and (B) CVs of HRP-NpAc-IL/GCE and HRP-NpAc-IL/MWCNT/GCE obtained for different concentrations of H_2O_2 at a scan rate of 50 mV s^{-1}. Inset: CVs of (A) Bare GCE and (B) MWCNT/GCE and NpAc-IL/MWCNT/GCE in the absence and presence of 0.5 mM H_2O_2 respectively. (C) Amperometry response for HRP-NpAc-IL/GCE (Red) and HRP-NpAc-IL/MWCNT/GCE (Blue) on successive additions of H_2O_2. (D) A plot of electrocatalytic current vs. concentration of H_2O_2. Electrolyte: N_2 saturated 0.1 M phosphate buffer (pH 7.0).

200 mV s^{-1} in N_2 saturated phosphate buffer (Fig. S7). On increasing the scan rate, there was a linear increase in both the peak currents without any noticeable change in the peak potentials, which signifies a surface confined redox process. The total amount of charge (Q) passed or liberated through the modified electrode during the redox process of HRP was obtained by integrating the CV peak of HRP-NpAc-IL/MWCNT/GCE in Fig. 4B. Using Faraday's law, the average surface coverage (Γ^*) of electroactive HRP in the biosensor was estimated to be 8.51×10^{-11} mol cm^{-2} from the equation, $\Gamma^* = Q/nFA$ (A = electrode area; n = no. of electrons involved; F = Faraday constant (96,485 C mol^{-1})), which is ~1.7 times larger than the theoretical monolayer coverage (5×10^{-11} mol cm^{-2}) for the immobilized HRP [49]. Thus, HRP was sequentially immobilized over the NpAc-IL/MWCNT/GCE platform, which is ascribed to the covalent anchoring of HRP on NpAc-IL moiety.

After successful characterization of the fabricated biosensor, it was then utilized for the electrocatalytic reduction of H_2O_2 in N_2 saturated 0.1 M phosphate buffer solution. Fig. 5A shows the CV responses of HRP-NpAc-IL/GCE for the sequential additions of H_2O_2 (0.1, 0.2, 0.3, 0.4, 0.5, 0.6 mM) concentrations at 50 mV s^{-1} and the red curve denotes the CV of HRP-NpAc-IL/GCE in the absence of H_2O_2. After the addition of H_2O_2, immediate increase in the cathodic peak current of HRP was observed, which signifies the electrocatalytic reduction of H_2O_2 at the developed biosensor [50]. When H_2O_2 is added to the electrolyte, the reduced form of HRP, i.e., HRP (Fe^{II}) reduces H_2O_2 available on the electrode surface and gets oxidised back to HRP (Fe^{III}) as shown in Eq. (2) [51]. This HRP (Fe^{III}) in turn immediately gets reduced to HRP (Fe^{II}) as presented in Eq. (1) and these reactions proceed in a cycle as long as H_2O_2 is available on the electrode surface, resulting in enhanced cathodic peak current. The increase in cathodic current is directly proportional to the concentration of H_2O_2 added into the electrolyte. On the other hand, bare GCE (inset to Fig. 5A), MWCNT/GCE and NpAc-IL/MWCNT/GCE (inset to Fig. 5B) showed a relatively feeble current response at a higher reduction potential for the addition of 0.5 mM H_2O_2. These observations further confirm the high electrocatalytic behaviour of the developed biosensor, which could be attributed to the effective covalent linking of HRP as well as high conducting nature of the newly developed NpAc-IL/GCE platform. Incorporation of MWCNT into the biosensor setup (HRP-NpAc-IL/MWCNT/GCE), tremendously increased the cathodic peak current for the same concentrations of H_2O_2 (Fig. 5B), which attributes to the synergistic effect of π-π stacked MWCNT on the NpAc-IL network and augment the conductivity [52].

$$\mathrm{HRP}\left(\mathrm{Fe^{II}}\right) + \mathrm{H_2O_2} + 2\mathrm{H^+} \rightarrow \mathrm{HRP}\left(\mathrm{Fe^{III}}\right) + 2\mathrm{H_2O} \quad (2)$$

Further, amperometry was performed at an applied potential of −0.4 V under dynamic conditions by constantly stirring (350 rpm) the electrolyte solution with a magnetic stirrer and incremental

Table 1
Comparison of performances of various enzymatic H_2O_2 biosensors.

Electrodes	Linear range (mM)	Sensitivity ($\mu A\ mM^{-1}\ cm^{-2}$)	LOD (μM)	Ref.
Cyt c-PAN-PDA/GCE	0.02–0.38	24	7.3	[53]
HRP-OANWs	0.02–0.5	31	5	[54]
HRP/ZnO-AuNp-Nf/GCE	0.015–1.1	–	9	[48]
HRP-Fe_3O_4/CS-GC	0.2–12	9.38	100	[55]
HRP/GA/PAMAM/CtRGO/GCE	0.05–0.8	29.86	25	[56]
HRP/ERGO/SPCE	0.009–0.195	90	–	[57]
HRP/polyAuNP/Au	0.005–1.1	0.498	1.5	[58]
HRP-AuNPs-SF/GCE	0.01–1.8	–	5	[59]
HRP-NpAc-IL/MWCNT/GCE	0.01–2.07	55.98	2.7	This work

additions of H_2O_2 were spiked into the electrolyte solution (Fig. 5C). For every addition, HRP-NpAc-IL/MWCNT/GCE showed an instantaneous increase in the catalytic current and the response current gets stabilized within less than 3 s, which depicts the rapid response of the fabricated biosensor towards reduction of H_2O_2. Although, HRP-NpAc-IL/GCE also showed catalytic current, the obtained response was very less for the same concentrations of H_2O_2, denoting the higher conducting nature of the NpAc-IL/MWCNT/GCE platform due to the complementary behaviour of NpAc-IL over MWCNT. On plotting current versus concentration of H_2O_2, a linear range of 0.01 to 2.07 mM with sensitivities of 55.98 & 29.79 $\mu A\ mM^{-1}\ cm^{-2}$ and detection limits of 2.7 & 6.2 μM for HRP-NpAc-IL/MWCNT/GCE and HRP-NpAc-IL/GCE were obtained respectively (Fig. 5D). The attained analytical parameters were comparable or better than the recently reported literatures and the data are shown in Table 1.

3.4. Stability, selectivity and reproducibility of HRP-NpAc-IL/MWCNT/GCE

The cyclic stability of the developed biosensor was accessed by performing 50 continuous potential cycles in N_2 saturated 0.1 M phosphate buffer solution at a scan rate of 50 mV s^{-1} (Fig. 6A). Thus, obtained voltammograms were highly stable even after 50 continuous scans without any change in the peak behaviour, which denotes the high stability of the immobilized HRP in the fabricated biosensor. Further, the long-term storage stability of the developed biosensor was investigated for 30 days in the absence as well as presence of 0.5 mM H_2O_2 under similar condition (Fig. 6B). Even after 30 days the biosensor could retain 94.2% and 92.5% of its initial current response in the absence as well as presence of H_2O_2 respectively. This enhanced stability of the developed biosensor could be attributed to the stable covalent immobilization of water soluble HRP enzyme on the favourable

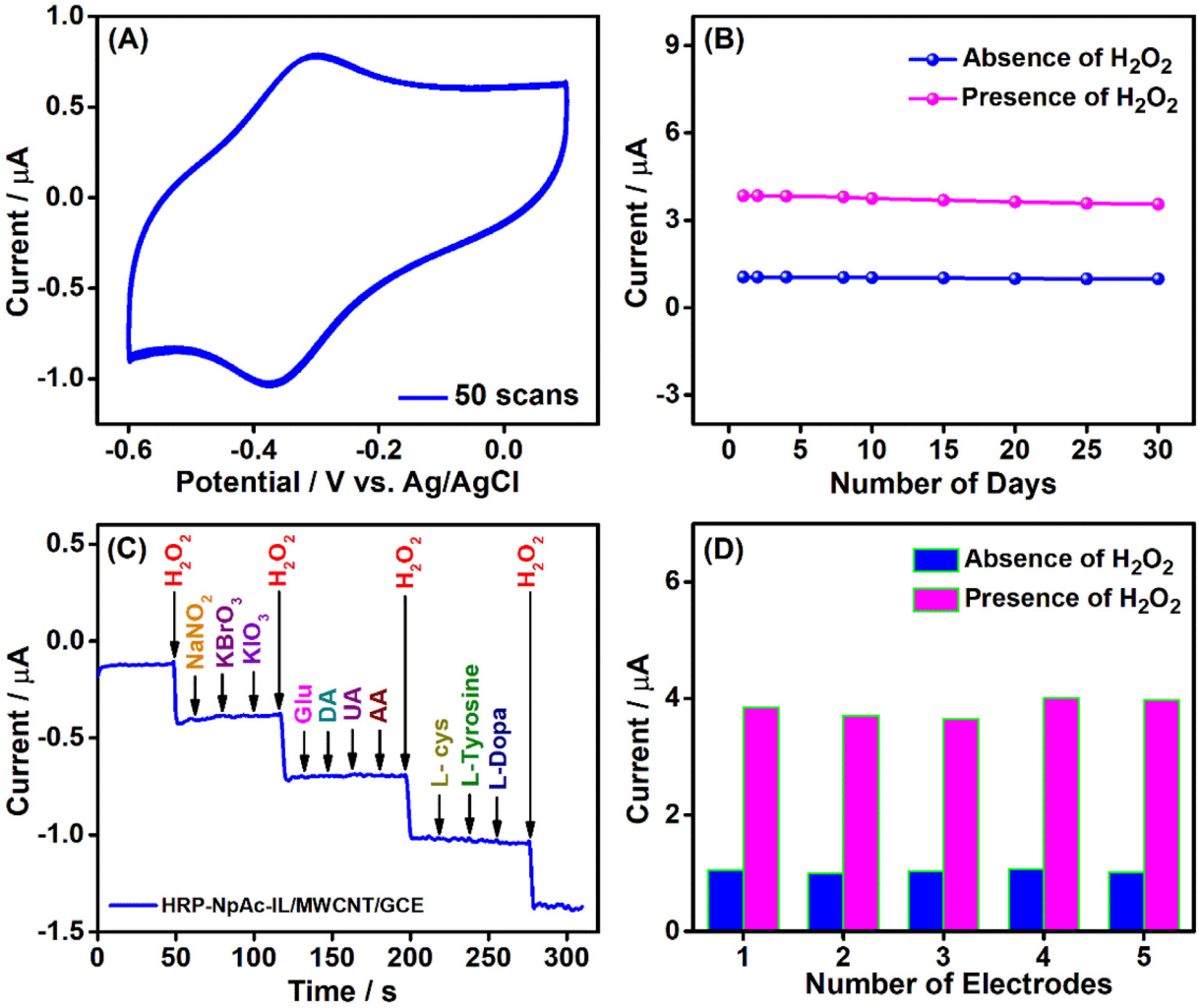

Fig. 6. (A) CVs of HRP-NpAc-IL/MWCNT/GCE (50 continuous cycles) at 50 mV s^{-1}. (B) Current response of HRP-NpAc-IL/GCE over 30 days in the absence and presence of H_2O_2 (C) Selectivity study of HRP-NpAc-IL/MWCNT/GCE for the sequential additions of 0.1 mM H_2O_2 and 1 mM of common co-existing species by amperometry. (D) Bar diagram of current responses obtained with 5 independently developed HRP-NpAc-IL/MWCNT/GCE without (blue) and with (pink) 0.5 mM H_2O_2. Electrolyte: N_2 saturated 0.1 M phosphate buffer (pH 7.0).

microenvironment of naphthyl substituted acetate functionalized ionic liquid through the amide bond.

The selectivity of the developed biosensor was tested for the commonly interfering as well as co-existing electroactive analytes by amperometry in a constantly stirred 0.1 M phosphate buffer (Fig. 6C). For every addition of 0.1 mM H_2O_2, there was an immediate increase in the catalytic current, but no change in current was observed for even 10-fold excess concentrations of interferents such as $NaNO_2$, $KBrO_3$, KIO_3, glucose (Glu), dopamine (DA), uric acid (UA), ascorbic acid (AA), L-cystine (L-cys), L-tyrosine and L-dopa, which shows the high selectivity of the fabricated biosensor. Reproducibility studies were performed for five individually fabricated biosensors and their performance in the absence as well as presence of 0.5 mM H_2O_2 under aforementioned conditions was tested and shown in Fig. 6D. The fabricated biosensor showed excellent reproducibility with the individually developed biosensors having an RSD value of 2.94% and 4.08% in the absence and presence of H_2O_2 respectively.

3.5. Determination of H_2O_2 in real systems

The proposed biosensor was evaluated for its applicability in the detection and estimation of H_2O_2 spiked in real samples like human serum and whole milk. The obtained serum and milk samples were diluted using phosphate buffer (0.1 M, pH 7.0) and known concentrations of H_2O_2 were spiked using standard addition method and the amperometric response was shown in Fig. S8. The recoveries were obtained in the range of 98.8% to 103.2% as shown in Table 2. The obtained results indicate the suitability of the developed biosensor for the analysis of H_2O_2 in real samples, which could be attributed to the high sensitivity, selectivity, rigidity and facile fabrication methodology of the proposed HRP-NpAc-IL/MWCNT/GCE biosensor.

4. Conclusions

Herein, we report a highly facile and stable anchoring platform for the direct and effective covalent anchoring of HRP enzyme without any crosslinker. The scaffold encompasses of a naphthyl group containing acetate functionalized ionic liquid (NpAc-IL) over MWCNT coated GCE surface. The -OCH_3 group of NpAc-IL was effectively used for the covalent immobilization of HRP via amide bond formation, whereas the naphthalene group was utilized for the π-π stacking with the MWCNT network. The enhanced conductivity and high stability of developed biosensor even in the dynamic conditions is due to the covalent linking of HRP on a highly conducting, biocompatible NpAc-IL along with the synergistic behaviour of MWCNT. This biosensor set up afforded promising performance towards H_2O_2 detection, besides excellent recovery in complex real samples. Hence, the newly developed NpAc-IL/MWCNT matrix elicits diverse approaches in the design and development of various bioanalytical devices, where the stable and efficacious immobilization of biomolecules remains a daunting challenge.

Credit author statement

K Theyagarajan: Investigation, Methodology, Validation, Writing – original draft. **Mari Elancheziyan**: Investigation, Validation. **Prakash Sinha Aayushi**: Methodology, Writing - original draft. **Kathavarayan Thenmozhi**: Conceptualization, Writing - review & editing, Project administration, Supervision.

Table 2
Detection of H_2O_2 spiked in real samples.

Sample	Spiked (mM)	Found (mM)	Recovery (%)	RSD[a] (%)
Human serum	0.25	0.258	103.2	3.1
	0.35	0.346	98.8	2.9
Whole milk	0.50	0.509	101.8	2.1
	0.70	0.712	101.7	1.8

[a] Triplicates were performed.

Declaration of competing interest

The authors declare that they have no known competing financial interests or personal relationships that could have appeared to influence the work reported in this paper.

Acknowledgement

The authors sincerely acknowledge the Science and Engineering Research Board (SERB), Government of India (Sanction No. SB/FT/CS-018/2014), for the financial assistance. The authors are grateful to Vellore Institute of Technology (VIT) for providing 'VIT SEED GRANT' for carrying out this research.

Appendix A. Supplementary data

Supplementary data to this article can be found online at https://doi.org/10.1016/j.ijbiomac.2020.07.005.

References

[1] M. Eguílaz, R. Villalonga, G. Rivas, Electrochemical biointerfaces based on carbon nanotubes-mesoporous silica hybrid material: bioelectrocatalysis of hemoglobin and biosensing applications, Biosens. Bioelectron. 111 (2018) 144–151, https://doi.org/10.1016/j.bios.2018.04.004.
[2] Y. Zhang, Q. Wei, The role of nanomaterials in electroanalytical biosensors: a mini review, J. Electroanal. Chem. 781 (2016) 401–409, https://doi.org/10.1016/j.jelechem.2016.09.011.
[3] C. Zhang, L. Li, J. Ju, W. Chen, Electrochemical sensor based on graphene-supported tin oxide nanoclusters for nonenzymatic detection of hydrogen peroxide, Electrochim. Acta 210 (2016) 181–189, https://doi.org/10.1016/j.electacta.2016.05.151.
[4] E.T.S.G. da Silva, D.E.P. Souto, J.T.C. Barragan, J. de F. Giarola, A.C.M. de Moraes, L.T. Kubota, Electrochemical biosensors in point-of-care devices: recent advances and future trends, ChemElectroChem 4 (2017) 778–794, https://doi.org/10.1002/celc.201600758.
[5] S.A.N. Gowers, V.F. Curto, C.A. Seneci, C. Wang, S. Anastasova, P. Vadgama, G.Z. Yang, M.G. Boutelle, 3D printed microfluidic device with integrated biosensors for online analysis of subcutaneous human microdialysate, Anal. Chem. 87 (2015) 7763–7770, https://doi.org/10.1021/acs.analchem.5b01353.
[6] T. Gan, S. Hu, Electrochemical sensors based on graphene materials, Microchim. Acta 175 (2011) 1–19, https://doi.org/10.1007/s00604-011-0639-7.
[7] S. Verma, J. Choudhary, K.P. Singh, P. Chandra, S.P. Singh, Uricase grafted nanoconducting matrix based electrochemical biosensor for ultrafast uric acid detection in human serum samples, Int. J. Biol. Macromol. 130 (2019) 333–341, https://doi.org/10.1016/j.ijbiomac.2019.02.121.
[8] K. Balasubramanian, M. Burghard, Biosensors based on carbon nanotubes, Anal. Bioanal. Chem. 385 (2006) 452–468, https://doi.org/10.1007/s00216-006-0314-8.
[9] X. Liu, J. Zhang, S. Liu, Q. Zhang, X. Liu, D.K.Y. Wong, Gold nanoparticle encapsulated-tubular TiO_2 nanocluster as a scaffold for development of thiolated enzyme biosensors, Anal. Chem. 85 (2013) 4350–4356, https://doi.org/10.1021/ac303420a.
[10] S. Alim, A.K.M. Kafi, J. Rajan, M.M. Yusoff, Application of polymerized multiporous nanofiber of SnO_2 for designing a bienzyme glucose biosensor based on HRP/GOx, Int. J. Biol. Macromol. 123 (2019) 1028–1034, https://doi.org/10.1016/j.ijbiomac.2018.11.171.
[11] X. Chen, G. Li, G. Zhang, K. Hou, H. Pan, M. Du, Self-assembly of palladium nanoparticles on functional TiO_2 nanotubes for a nonenzymatic glucose sensor, Mater. Sci. Eng. C 62 (2016) 323–328, https://doi.org/10.1016/j.msec.2016.01.068.
[12] C. Zhang, Y. Zhang, Z. Miao, M. Ma, X. Du, J. Lin, B. Han, S. Takahashi, J. Anzai, Q. Chen, Dual-function amperometric sensors based on poly(diallydimethylammoniun chloride)-functionalized reduced graphene oxide/manganese dioxide/gold nanoparticles nanocomposite, Sensors Actuators B Chem. 222 (2016) 663–673, https://doi.org/10.1016/j.snb.2015.08.114.
[13] C. Chen, Q. Xie, D. Yang, H. Xiao, Y. Fu, Y. Tan, S. Yao, Recent advances in electrochemical glucose biosensors: a review, RSC Adv. 3 (2013) 4473–4491, https://doi.org/10.1039/c2ra22351a.
[14] D.W. Kimmel, G. LeBlanc, M.E. Meschievitz, D.E. Cliffel, Electrochemical sensors and biosensors, Anal. Chem. 84 (2012) 685–707, https://doi.org/10.1021/ac202878q.
[15] M. Sharifi, M.J. Sohrabi, S.H. Hosseinali, A. Hasan, P.H. Kani, A.J. Talaei, A.Y. Karim, N.M.Q. Nanakali, A. Salihi, F.M. Aziz, B. Yan, R.H. Khan, A.A. Saboury, M. Falahati, Enzyme immobilization onto the nanomaterials: application in enzyme stability and prodrug-activated cancer therapy, Int. J. Biol. Macromol. 143 (2020) 665–676, https://doi.org/10.1016/j.ijbiomac.2019.12.064.

[16] M. Sharifi, A.Y. Karim, N. Mustafa Qadir Nanakali, A. Salihi, F.M. Aziz, J. Hong, R.H. Khan, A.A. Saboury, A. Hasan, O.K. Abou-Zied, M. Falahati, Strategies of enzyme immobilization on nanomatrix supports and their intracellular delivery, J. Biomol. Struct. Dyn. 38 (2020) 2746–2762, https://doi.org/10.1080/07391102.2019.1643787.
[17] S.A. Mohamed, A.L. Al-Malki, T.A. Kumosani, R.M. El-Shishtawy, Horseradish peroxidase and chitosan: activation, immobilization and comparative results, Int. J. Biol. Macromol. 60 (2013) 295–300, https://doi.org/10.1016/j.ijbiomac.2013.06.003.
[18] S.A. Mohamed, S.S. Al-Ghamdi, R.M. El-Shishtawy, Immobilization of horseradish peroxidase on amidoximated acrylic polymer activated by cyanuric chloride, Int. J. Biol. Macromol. 91 (2016) 663–670, https://doi.org/10.1016/j.ijbiomac.2016.06.002.
[19] Y.Q. Almulaiky, R.M. El-Shishtawy, M. Aldhahri, S.A. Mohamed, M. Afifi, W.H. Abdulaal, J.A. Mahyoub, Amidrazone modified acrylic fabric activated with cyanuric chloride: a novel and efficient support for horseradish peroxidase immobilization and phenol removal, Int. J. Biol. Macromol. 140 (2019) 949–958, https://doi.org/10.1016/j.ijbiomac.2019.08.179.
[20] J. Ge, J. Lei, R.N. Zare, Protein-inorganic hybrid nanoflowers, Nat. Nanotechnol. 7 (2012) 428–432, https://doi.org/10.1038/nnano.2012.80.
[21] J. Sun, J. Ge, W. Liu, M. Lan, H. Zhang, P. Wang, Y. Wang, Z. Niu, Multi-enzyme co-embedded organic-inorganic hybrid nanoflowers: synthesis and application as a colorimetric sensor, Nanoscale 6 (2014) 255–262, https://doi.org/10.1039/c3nr04425d.
[22] B. Somturk, M. Hancer, I. Ocsoy, N. Özdemir, Synthesis of copper ion incorporated horseradish peroxidase-based hybrid nanoflowers for enhanced catalytic activity and stability, Dalton Trans. 44 (2015) 13845–13852, https://doi.org/10.1039/c5dt01250c.
[23] C. Altinkaynak, I. Yilmaz, Z. Koksal, H. Özdemir, I. Ocsoy, N. Özdemir, Preparation of lactoperoxidase incorporated hybrid nanoflower and its excellent activity and stability, Int. J. Biol. Macromol. 84 (2016) 402–409, https://doi.org/10.1016/j.ijbiomac.2015.12.018.
[24] C. Altinkaynak, S. Tavlasoglu, R. Kalin, N. Sadeghian, H. Ozdemir, I. Ocsoy, N. Özdemir, A hierarchical assembly of flower-like hybrid Turkish black radish peroxidase-Cu^{2+} nanobiocatalyst and its effective use in dye decolorization, Chemosphere 182 (2017) 122–128, https://doi.org/10.1016/j.chemosphere.2017.05.012.
[25] L.B. Wang, Y.C. Wang, R. He, A. Zhuang, X. Wang, J. Zeng, J.G. Hou, A new nanobiocatalytic system based on allosteric effect with dramatically enhanced enzymatic performance, J. Am. Chem. Soc. 135 (2013) 1272–1275, https://doi.org/10.1021/ja3120136.
[26] N. Ildiz, A. Baldemir, C. Altinkaynak, N. Özdemir, V. Yilmaz, I. Ocsoy, Self assembled snowball-like hybrid nanostructures comprising *Viburnum Opulus* L. extract and metal ions for antimicrobial and catalytic applications, Enzym. Microb. Technol. 102 (2017) 60–66, https://doi.org/10.1016/j.enzmictec.2017.04.003.
[27] A. Baldemir, N.B. Köse, N. Ildiz, S. İlgün, S. Yusufbeyoğlu, V. Yilmaz, I. Ocsoy, Synthesis and characterization of green tea (*Camellia sinensis* (L.) Kuntze) extract and its major components-based nanoflowers: a new strategy to enhance antimicrobial activity, RSC Adv. 7 (2017) 44303–44308, https://doi.org/10.1039/c7ra07618e.
[28] C. Celik, N. Ildiz, I. Ocsoy, Building block and rapid synthesis of catecholamines-inorganic nanoflowers with their peroxidase-mimicking and antimicrobial activities, Sci. Rep. 10 (2020) 2903, https://doi.org/10.1038/s41598-020-59699-5.
[29] J. Wang, Carbon-nanotube based electrochemical biosensors: a review, Electroanalysis 17 (2005) 7–14, https://doi.org/10.1002/elan.200403113.
[30] M.E. Ghica, R. Pauliukaite, O. Fatibello-Filho, C.M.A. Brett, Application of functionalised carbon nanotubes immobilised into chitosan films in amperometric enzyme biosensors, Sensors Actuators B Chem. 142 (2009) 308–315, https://doi.org/10.1016/j.snb.2009.08.012.
[31] S. Gupta, C.N. Murthy, C.R. Prabha, Recent advances in carbon nanotube based electrochemical biosensors, Int. J. Biol. Macromol. 108 (2018) 687–703, https://doi.org/10.1016/j.ijbiomac.2017.12.038.
[32] A. Kumar, M. Bisht, P. Venkatesu, Biocompatibility of ionic liquids towards protein stability: a comprehensive overview on the current understanding and their implications, Int. J. Biol. Macromol. 96 (2017) 611–651, https://doi.org/10.1016/j.ijbiomac.2016.12.005.
[33] P. Damlin, M. Suominen, M. Heinonen, C. Kvarnström, Non-covalent modification of graphene sheets in PEDOT composite materials by ionic liquids, Carbon 93 (2015) 533–543, https://doi.org/10.1016/j.carbon.2015.05.055.
[34] P. Hapiot, C. Lagrost, Electrochemical reactivity in room-temperature ionic liquids, Chem. Rev. 108 (2008) 2238–2264, https://doi.org/10.1021/cr0680686.
[35] R. Giernoth, Task-specific ionic liquids, Angew. Chem. Int. Ed. 49 (2010) 2834–2839, https://doi.org/10.1002/anie.200905981.
[36] W. Lan, C.F. Liu, F.X. Yue, R.C. Sun, J.F. Kennedy, Ultrasound-assisted dissolution of cellulose in ionic liquid, Carbohydr. Polym. 86 (2011) 672–677, https://doi.org/10.1016/j.carbpol.2011.05.013.
[37] K. Kwak, S. Senthilkumar, K. Pyo, D. Lee, Ionic liquid of a gold nanocluster: a versatile matrix for electrochemical biosensors, ACS Nano 8 (2014) 671–679, https://doi.org/10.1021/nn4053217.
[38] D.S. Silvester, Recent advances in the use of ionic liquids for electrochemical sensing, Analyst 136 (2011) 4871–4882, https://doi.org/10.1039/c1an15699c.
[39] R. Pauliukaite, A.P. Doherty, K.D. Murnaghan, C.M.A. Brett, Application of some room temperature ionic liquids in the development of biosensors at carbon film electrodes, Electroanalysis 20 (2008) 485–490, https://doi.org/10.1002/elan.200704081.
[40] K. Theyagarajan, D. Saravanakumar, S. Senthilkumar, K. Thenmozhi, Rationally designed naphthyl substituted amine functionalized ionic liquid platform for covalent immobilization and direct electrochemistry of hemoglobin, Sci. Rep. 9 (2019), 10428. https://doi.org/10.1038/s41598-019-46982-3.
[41] M. Murphy, K. Theyagarajan, P. Ganesan, S. Senthilkumar, K. Thenmozhi, Electrochemical biosensor for the detection of hydrogen peroxide using cytochrome c covalently immobilized on carboxyl functionalized ionic liquid/multiwalled carbon nanotube hybrid, Appl. Surf. Sci. 492 (2019) 718–725, https://doi.org/10.1016/j.apsusc.2019.06.283.
[42] W. Chen, S. Cai, Q.Q. Ren, W. Wen, Y. Di Zhao, Recent advances in electrochemical sensing for hydrogen peroxide: a review, Analyst 137 (2012) 49–58, https://doi.org/10.1039/c1an15738h.
[43] R. Zhang, W. Chen, Recent advances in graphene-based nanomaterials for fabricating electrochemical hydrogen peroxide sensors, Biosens. Bioelectron. 89 (2017) 249–268, https://doi.org/10.1016/j.bios.2016.01.080.
[44] X. Liu, H. Feng, J. Zhang, R. Zhao, X. Liu, D.K.Y. Wong, Hydrogen peroxide detection at a horseradish peroxidase biosensor with a Au nanoparticle-dotted titanate nanotube|hydrophobic ionic liquid scaffold, Biosens. Bioelectron. 32 (2012) 188–194, https://doi.org/10.1016/j.bios.2011.12.002.
[45] M. Feizabadi, A. Soleymanpour, H. Faridnouri, D. Ajloo, Improving stability of biosensor based on covalent immobilization of horseradish peroxidase by γ-aminobutyric acid and application in detection of H_2O_2, Int. J. Biol. Macromol. 136 (2019) 597–606, https://doi.org/10.1016/j.ijbiomac.2019.06.103.
[46] J. Cao, G. Xu, P. Li, M. Tao, W. Zhang, Polyacrylonitrile fiber supported N-heterocyclic carbene Ag(I) as efficient catalysts for three-component coupling and intramolecular 1,3-dipolar cycloaddition reactions under flow conditions, ACS Sustain. Chem. Eng. 5 (2017) 3438–3447, https://doi.org/10.1021/acssuschemeng.7b00103.
[47] Y. Niu, J. Liu, W. Chen, C. Yin, W. Weng, X. Li, X. Wang, G. Li, W. Sun, A direct electron transfer biosensor based on a horseradish peroxidase and gold nanotriangle modified electrode and electrocatalysis, Anal. Methods 10 (2018) 5297–5304, https://doi.org/10.1039/c8ay01980k.
[48] C. Xiang, Y. Zou, L.X. Sun, F. Xu, Direct electrochemistry and enhanced electrocatalysis of horseradish peroxidase based on flowerlike ZnO-gold nanoparticle-Nafion nanocomposite, Sensors Actuators B Chem. 136 (2009) 158–162, https://doi.org/10.1016/j.snb.2008.10.058.
[49] J. Li, S. Dong, The electrochemical study of oxidation-reduction properties of horseradish peroxidase, J. Electroanal. Chem. 431 (1997) 19–22, https://doi.org/10.1016/S0022-0728(97)00158-7.
[50] F. Li, Y. Feng, Z. Wang, L. Yang, L. Zhuo, B. Tang, Direct electrochemistry of horseradish peroxidase immobilized on the layered calcium carbonate-gold nanoparticles inorganic hybrid composite, Biosens. Bioelectron. 25 (2010) 2244–2248, https://doi.org/10.1016/j.bios.2010.03.006.
[51] B. Wang, J.J. Zhang, Z.Y. Pan, X.Q. Tao, H.S. Wang, A novel hydrogen peroxide sensor based on the direct electron transfer of horseradish peroxidase immobilized on silica-hydroxyapatite hybrid film, Biosens. Bioelectron. 24 (2009) 1141–1145, https://doi.org/10.1016/j.bios.2008.06.053.
[52] M. Wang, Y. Gao, J. Zhang, J. Zhao, Highly dispersed carbon nanotube in new ionic liquid-graphene oxides aqueous dispersions for ultrasensitive dopamine detection, Electrochim. Acta 155 (2015) 236–243, https://doi.org/10.1016/j.electacta.2014.12.114.
[53] L. Zhang, Z. Shi, Q. Lang, J. Pan, Electrochemical synthesis of belt-like polyaniline network on *p*-phenylenediamine functionalized glassy carbon electrode and its use for the direct electrochemistry of horse heart cytochrome c, Electrochim. Acta 55 (2010) 641–647, https://doi.org/10.1016/j.electacta.2009.09.017.
[54] E. Koposova, X. Liu, A. Kisner, Y. Ermolenko, G. Shumilova, A. Offenhäusser, Y. Mourzina, Bioelectrochemical systems with oleylamine-stabilized gold nanostructures and horseradish peroxidase for hydrogen peroxide sensor, Biosens. Bioelectron. 57 (2014) 54–58, https://doi.org/10.1016/j.bios.2014.01.034.
[55] X. Tan, J. Zhang, S. Tan, D. Zhao, Z. Huang, Y. Mi, Z. Huang, Amperometric hydrogen peroxide biosensor based on horseradish peroxidase immobilized on Fe_3O_4/Chitosan modified glassy carbon electrode, Electroanalysis 21 (2009) 1514–1520, https://doi.org/10.1002/elan.200804572.
[56] C.S. Rao Vusa, V. Manju, S. Berchmans, P. Arumugam, Electrochemical amination of graphene using nanosized PAMAM dendrimers for sensing applications, RSC Adv. 6 (2016) 33409–33418, https://doi.org/10.1039/c5ra27862g.
[57] S. Palanisamy, B. Unnikrishnan, S.M. Chen, An amperometric biosensor based on direct immobilization of horseradish peroxidase on electrochemically reduced graphene oxide modified screen printed carbon electrode, Int. J. Electrochem. Sci. 7 (2012) 7935–7947.
[58] R. Villalonga, P. Díez, P. Yáñez-Sedeño, J.M. Pingarrón, Wiring horseradish peroxidase on gold nanoparticles-based nanostructured polymeric network for the construction of mediatorless hydrogen peroxide biosensor, Electrochim. Acta 56 (2011) 4672–4677, https://doi.org/10.1016/j.electacta.2011.02.108.
[59] H. Yin, S. Ai, W. Shi, L. Zhu, A novel hydrogen peroxide biosensor based on horseradish peroxidase immobilized on gold nanoparticles-silk fibroin modified glassy carbon electrode and direct electrochemistry of horseradish peroxidase, Sensors Actuators B Chem. 137 (2009) 747–753, https://doi.org/10.1016/j.snb.2008.12.046.